PAPER Nr.: 70

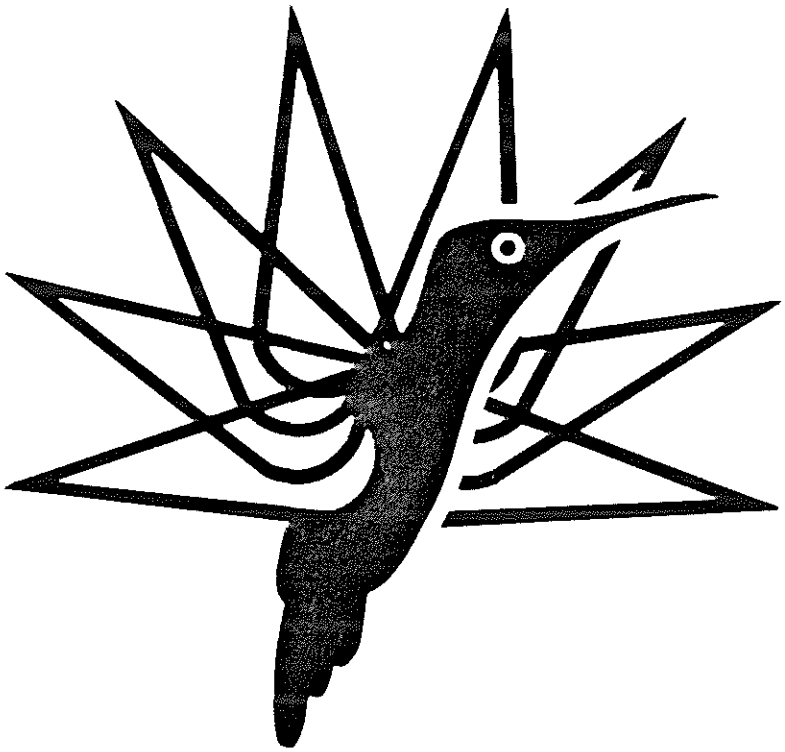

THE INFLUENCE OF THE ROTOR WAKE ON ROTORCRAFT STABILITY AND CONTROL

by

H. C. CURTISS, JR.
PRINCETON UNIVERSITY

T. R. QUACKENBUSH
CONTINUUM DYNAMICS, INC.
PRINCETON, NJ, U.S.A.

FIFTEENTH EUROPEAN ROTORCRAFT FORUM

SEPTEMBER 12 - 15, 1989 AMSTERDAM

THE INFLUENCE OF THE ROTOR WAKE ON ROTORCRAFT STABILITY AND CONTROL

H. C. Curtiss, Jr.
Princeton University

and

T. R. Quackenbush
Continuum Dynamics, Inc.
Princeton, NJ

ABSTRACT

The effect of the time-averaged rotor wake flow field on the aerodynamic behavior of the tail rotor and fixed tail surfaces is discussed. The flow field at the location of these surfaces is predicted by two wake models, a simplified flat wake model and an accurate free wake model. Both models are shown to give similar predictions of the flow field in the vicinity of the empennage that are generally in agreement with experiment. The contributions of these aerodynamic interactions to the helicopter stability derivatives are described and control responses using different wake models are compared with flight test.

1. Introduction

Contemporary helicopters have relatively large fixed tail surfaces as well as a tail rotor operating in the complex wake of the main rotor. Larger horizontal tail surfaces generally result from a requirement to provide inherent angle of attack stability [1] or at least to counter some of the main rotor instability at high forward speeds. Vertical tail surfaces generally reflect a design requirement to make the body vertical-tail combination directionally stable. A number of undesirable or poorly understood effects arise from the interaction of these surfaces and the main rotor wake both at low speeds and at high speeds. This paper examines some of these effects, which are often characterized as interactional aerodynamics, at reasonably high translational speeds. There seems to be a tendency to categorize many phenomena placed under the heading of interactional aerodynamics as arising from somewhat mysterious sources using physical reasoning that is not generally in accord with theory. This paper discusses quantitatively the wake characteristics and their effects on the tail surface and tail rotor aerodynamics. A relatively simple wake model appears to give a quite suitable description of the rotor wake in translational flight . This model from Reference 2 is briefly described along with the predicted flow field downstream of the rotor. Reference 2 indicates that this model predicts wake characteristics that are generally in

agreement with experiment, certainly in a qualitative sense if not in a quantitative sense. The influence of the flow field predicted by this wake model on the aerodynamics of the horizontal tail, the vertical tail and tail rotor is examined. Attention is directed towards lateral-longitudinal coupling effects which have been noted to give rise to a variety of handling qualities problems [1,3,4]. The flow field predictions of the simple wake model are compared with a more accurate free wake model that has been shown to produce very good agreement with experimental measurements for rotor blade airloads in translational flight as well as for the wake flow field [5]. Finally, the importance of some of these effects on helicopter response to control inputs is shown and compared with flight test.

2. Discussion

In general the main rotor wake has components in all three directions in the vicinity of the horizontal tail, vertical tail and tail rotor. Prediction of these components generally involve very complex models for the rotor wake. However a particularly interesting and relatively simple model for the rotor wake is given in Reference 2 where it is also shown to give predictions of the rotor flow field especially as regards downwash and sidewash downstream of the rotor that agree quite well with experiment. This theory is generally simple enough to be incorporated into a complex flight dynamics program. Basically the theory is the rotating wing analog of Prandtl's finite wing theory. The vortex wake is assumed to be transported downstream in the direction of the freestream velocity with no distortion and thus is referred to in this paper as the flat wake theory. Due to this assumption its use is restricted to reasonable translational flight velocities. The vortices leaving the trailing edge of the blades are assumed to move downstream in cycloids whose shape is determined by the advance ratio and local radius. This cycloidal pattern of vortex lines is then smeared into a vortex sheet which is used to calculate the rotor flow field by means of the Biot-Savart Law. The wake characteristics are assumed to be time invariant and the vorticity distribution in the wake is based on a radial blade circulation distribution that is independent of azimuth. The cycloidal shape of the vorticity in the wake results in considerable asymmetry even though there is no asymmetry in the airload. The blade circulation distribution with radius is assumed with an integrated value corresponding to main rotor thrust. The version of this theory used in the paper is the complete theory as presented in Reference 2 rather than the simpler far wake results which were used in a previous study (Reference 6). Considerable improvement in the prediction of the control response of a UH-60A helicopter was shown by incorporating this model into the prediction of the interaction of the main rotor wake with the tail surfaces and tail rotor. The latter part of this paper discusses the influence of these terms on the response in some detail as

they are of primary significance in the translational flight control responses.

Flow Field

In general at the fixed tail surfaces and the tail rotor, the main rotor will induce velocity components in all three directions, i.e., downwash, sidewash, and inplane wash. The coordinate system is shown in Figure 1. The distribution of these three components normalized by the momentum value of the induced velocity along the lateral axis as predicted by the relatively simple flat wake model of Reference 2 are shown in Figure 2 in the region of the horizontal tail. The vertical distribution is shown in Figure 3. These results generally agree with experiment as shown in Reference 2. The advance ratio is 0.2. The geometry corresponds to a UH-60 helicopter at 86 kts. These calculations are based on the assumption of a circulation distribution on the blades that is independent of azimuth and has a cubic variation with radius. The downwash pattern in Figure 2 shows the well established fact that the downwash velocity is larger on the advancing side of the rotor relative to the retreating side. Note that this pattern is essentially a result of the cycloidal shape of the wake and not to any more complex feature of the rotor aerodynamics such as the reverse flow region. The sidewash distribution shown in Figure 3 indicates a significant component towards the advancing side above the plane of the wake and towards the retreating side of the rotor below the wake. The inplane wash as shown in Figure 3 is upstream below the rotor wake and downstream above the wake. These velocity distributions provide a suitable basis for discussion of effects on the tail surfaces. The advance ratio dependence of these distributions is as follows. The sidewash velocity normalized by the momentum value of the induced velocity is proportional to advance ratio. The symmetric part of the normalized downwash velocity is independent of advance ratio and the asymmetric part is proportional to advance ratio. Comparison and discussion of this predicted flow field with a more accurate free wake model of the rotor wake is discussed later in the paper. The general features of the flow field shown in Figures 2 and 3 appear to be a basic characterization of the average rotor wake flow field. While the precise numerical values on the curves will depend in some detail on the rotor wake model, the general shape of the curves is primarily due to the cycloidal nature of the wake. Sensitivities are discussed in a later section.

The inplane wash is not considered further although in general it will have the effect of reducing the dynamic pressure at low tail locations and increasing the dynamic pressure at high tail locations and is accounted for in the dynamic model of the helicopter.

The primary influence of the downwash will be on the horizontal tail and the sidewash will influence the

aerodynamics of the vertical tail and tail rotor.

In general, as the angle of attack and the sideslip of the rotorcraft vary, the wake pattern will move relative to the tail surfaces as shown in Figure 1, producing changes in the forces and moments acting on these surfaces. In addition to this geometric displacement, the main rotor thrust will change with main rotor angle of attack causing a proportional variation in the wake velocity components. In steady flight, the symmetric part of the downwash distribution will produce a steady lift on the horizontal tail and the asymmetric part will produce a steady rolling moment. Sideslip of the aircraft will result in lateral displacement of this wake pattern and it can be shown that the anti-symmetric part of the distribution will produce a linear variation of the lift on the horizontal tail with sideslip. Displacement of the symmetric part of the distribution will produce a linear variation in rolling moment. Thus in addition to trim moments, the downwash distribution in Figure 2 will result in a horizontal tail lift variation with sideslip and consequently a pitching moment variation as well as a rolling moment variation with sideslip. Nonlinear effects are also produced. Dominant nonlinear effects result from opposite components, i.e., deflection of an anti-symmetric distribution produces a nonlinear contribution to the rolling moment and deflection of the symmetric distribution causes a nonlinear variation in the lift. Both of these nonlinear effects are moderately important.

In addition to these displacement effects there are also effects which can be termed gradient effects which in the case of the horizontal tail are due to angle of attack variation. Calculations indicate that for the flat wake model, these gradient effects do not result in large variations with the other coordinate, that is, the downwash is approximately a product of two functions and the gradient is approximated by the centerline variation. The gradient effects associated with angle of attack combine with the effect of thrust variation which produces an increase in the magnitude of the downwash, i.e., the downwash normalized by the momentum value of the induced velocity is independent of thrust.

The influence of sidewash on the vertical tail leads to similar effects as described for the horizontal tail. However in this case, variation in angle of attack produces displacement effects which combines with downwash variations with thrust to produce coupling terms i.e., variation in tail sideforce and rolling moment with angle of attack. Sideslip produces a gradient effect which is moderately significant. The vertical distribution of sidewash looks very much like the flow field of a single line vortex and vertical displacement produces a relatively strong linear variation in the sideforce on the vertical tail when plane of the wake lies between the root and tip of the vertical tail. The slope changes significantly when the plane of the wake no longer intersects

the vertical tail.

The tail rotor also experiences this same flow field. In the case of the tail rotor, it is assumed that it is a flapping rotor and therefore that only the thrust force is of significance. The effects of the sidewash on the thrust of the tail rotor is estimated by determining the influence on each of four rotor blades, in vertical and horizontal locations, and averaging the results. Note that this sidewash field will produce a change in the steady state power required by the tail rotor as well as the tail rotor collective required for trim. In general, in powered high speed flight with a negative trim angle of attack the tail rotor would tend to be in the upper half of the flow field. Thus the tail rotor would experience a relative up-flow reducing the power required for a given thrust, as well as reducing the tail rotor pitch require to produce a certain thrust [2]. In descent, when the tail rotor is below the rotor wake, just the opposite would be the case, the tail rotor would experience a downflow. Consequently this causes an increase in tail rotor power and rudder pedal deflection. It is quite likely that the sidewash distribution contributes to the rather large discrepancy in rudder pedal position between theory and flight test shown in Reference 7 in descent.

Analytical expressions for the linearized effects of the downwash and sidewash distributions can be expressed as follows.

The lift coefficient of the horizontal tail and the sideforce coefficient of the vertical tail are:

$$C_{L_{HT}} = a_{HT}(\alpha - \tilde{\epsilon})$$

$$C_{Y_{VT}} = a_{VT}(\tilde{\sigma} - \beta)$$

The average sidewash and downwash for constant chord surfaces are defined as,

$$\tilde{\epsilon} = \frac{1}{2\bar{s}} \int_{-\bar{s}}^{\bar{s}} \epsilon(\bar{y}', \bar{z}')\, d\bar{z}$$

$$\tilde{\sigma} = \frac{1}{\bar{b}} \int_{o}^{\bar{b}} \sigma(\bar{y}', \bar{z}')\, d\bar{y}$$

The wake displacements due to angle of attack and sideslip are

$$\bar{z}' = \bar{z} + \bar{\ell}_T \beta$$

$$\bar{y}' = \bar{y} - \bar{\ell}_T \alpha$$

The downwash derivatives are therefore,

$$\frac{d\tilde{\epsilon}}{d\alpha} = \frac{1}{v_o} \frac{\partial v_o}{\partial \alpha} \tilde{\epsilon}_o - \bar{\ell}_T \frac{d\tilde{\epsilon}}{d\bar{y}}$$

$$\frac{d\tilde{\epsilon}}{d\beta} = \frac{\bar{\ell}_T}{2\bar{s}} [\epsilon(\bar{s}) - \epsilon(-\bar{s})]$$

The sidewash derivatives are

$$\frac{d\tilde{\sigma}}{d\alpha} = \frac{1}{v_o} \frac{\partial v_o}{\partial \alpha} \tilde{\sigma}_o - \frac{\bar{\ell}_T}{\bar{b}} [\sigma(\bar{b}) - \sigma(o)]$$

$$\frac{d\tilde{\sigma}}{d\beta} = \bar{\ell}_T \frac{d\tilde{\sigma}}{d\bar{z}}$$

The linearized expression for the displacement effects as given by the variation of downwash with sideslip and the second term in the variation of sidewash with angle of attack are particularly simple, depending only on the difference in downwash or sidewash components at each end of the surface of interest.

These are the linearized expressions. In general the variation in downwash with sideslip would be

$$\frac{d\tilde{\epsilon}}{d\beta} = \frac{\bar{\ell}_T}{2\bar{s}} [\epsilon(\bar{s} + \bar{\ell}_T \beta) - \epsilon(-\bar{s} + \bar{\ell}_T \beta)]$$

Expanding $\tilde{\epsilon}$ in a Taylor series

$$\frac{d\tilde{\epsilon}}{d\beta} = \frac{\bar{\ell}_T}{2\bar{s}} [\epsilon(\bar{s}) - \epsilon(-\bar{s}) + (\frac{d\epsilon}{d\bar{z}}(\bar{s}) - \frac{d\epsilon}{d\bar{z}}(-\bar{s}))\ \bar{\ell}_T \beta]$$

It can be seen from this expression that the linear effect depends upon the anti-symmetric character of the downwash and the first nonlinear term depends upon the symmetric character of the downwash.

Similar expressions can be formulated for the rolling moments produced by each surface. Only the linearized expression for the displacement effect on the horizontal tail is given.

The rolling moment coefficient can be expressed as

$$C_{\ell_{HT}} = a_{HT}(\tilde{\epsilon}z)$$

where

$$(\tilde{\epsilon}z) = \frac{1}{4\bar{s}^2} \int_{-\bar{s}}^{\bar{s}} \epsilon(\bar{y}', \bar{z}') \; \bar{z} \; d\bar{z}$$

so that

$$\frac{\partial C_{\ell_{HT}}}{\partial \beta} = a_{HT} \frac{\partial(\tilde{\epsilon}z)}{\partial \beta}$$

where $(\tilde{\epsilon}z)$ represents the weighted downwash averaged over the span. Then

$$\frac{d(\tilde{\epsilon}y)}{d\beta} = \frac{\bar{\ell}_T}{2\bar{s}} \left[\frac{\epsilon(\bar{s}) + \epsilon(-\bar{s})}{2} - \tilde{\epsilon}_o\right]$$

This expression shows clearly the linearized dependence of the rolling moment on the symmetric part of the distribution. Of course if the downwash is uniform across the surface ($\epsilon(\bar{s}) = \epsilon(-\bar{s}) = \tilde{\epsilon}_o$) then this term is zero. It should be noted that while these expressions appear to depend upon the loading at the tips of the blades they are in fact linearized expressions for the airload change across the span of the tail. These expression are useful for gaining physical insight into the important effects. Using a computer it is relatively straightforward to calculate the integrals involved directly. For simplicity, it has been assumed that the tail surfaces are of constant chord.

For tail rotor displacement effects, the expressions are somewhat more complex since the effect of a downwash distribution across the tail rotor on tail rotor thrust is weighted by the local radius of the blades.

The change in tail rotor thrust coefficient due to a sidewash distribution change

$$\Delta\left(\frac{2C_T}{a\sigma}\right) = \frac{\mu_{TR}}{2} (\tilde{\sigma}r)$$

where

$$(\tilde{\sigma}r) = \frac{2}{b_T} \frac{1}{\bar{R}_T^2} \int_o^{\bar{R}_T} \bar{r}\left(\sum_i^b \sigma_i\right) d\bar{r}$$

For a displacement in the flow field at the tail rotor, the change in the weighted average of the sidewash is

$$\left\{\frac{d\tilde{\sigma}_r}{d\alpha}\right\} = -\frac{2\bar{\ell}_T}{b_T \bar{R}_T}\left\{(\sigma(\bar{R}_T) - \tilde{\sigma}_o)_{\frac{\pi}{2}} - (\sigma(-\bar{R}_T) - \tilde{\sigma}_o)_{\frac{3\pi}{2}}\right.$$

$$\left. - \frac{1}{2}\frac{d\sigma}{d\bar{y}}_{o} - \frac{1}{2}\frac{d\sigma}{d\bar{y}}_{\pi}\right\}$$

The first two terms are due to the blades up and down in the field and the last two terms are due to the horizontal blades. For the last two terms the fore and aft variation of the sidewash is neglected. Note that $\tilde{\sigma}_o$ refers to an average not weighted by radius.

The up-down blades provide a contribution for an anti-symmetric distribution and of course for a uniform sidewash distribution there will be no thrust change produced. Note that the latter two terms will produce a significant nonlinearity for the sidewash distribution shown in Figure 3 when the initial position of the tail rotor is centered in the wake. The thrust variation due to these two blades will in fact vary just as the sidewash distribution and the first two contributions will be rather small. The tail rotor thrust variation will be quite non-linear for this sidewash distribution. The more refined model presented later softens this distribution and reduces the nonlinear behavior.

Numerical Results

In this section the general nature of the aerodynamic forces and moments produced by these downwash and sidewash components is examined. The focus is on the coupling effects, i.e., the effects caused by wake displacement resulting in horizontal tail forces varying with sideslip and vertical tail and tail rotor force variation with angle of attack. Again the flat wake results given in a previous section are used to present some sample results. The following are typical dimensions for the UH-60 tail surfaces and tail rotor all normalized by main rotor radius.

$$\bar{\ell}_T = -1.1$$

$$\bar{b} = 0.28$$

$$\bar{s} = 0.27$$

$$\bar{R}_{TR} = 0.21$$

These dimensions indicate the extent of the surfaces in the

flow fields shown in Figures 2 and 3 and also indicate that a sideslip of 10° for example will result in significant translation of the flow field relative to the surface.

First consider the effect of the downwash on the lift variation of the horizontal tail with sideslip. It is the downwash averaged across the span which produces a proportional change in lift on the horizontal tail. Figure 4 shows the variation in average downwash, normalized by the simple momentum value of the downwash angle. The linearized result shows the increasing downwash with positive slip resulting in a nose-up moment with positive slip. The dominant non-linear term is a squared effect showing that this coupling effect is stronger for positive slip than for negative slip [1]. There is however a reasonable range of linear behavior.

A rolling moment with slip is also produced. For this downwash distribution, the tendency is to produce a positive or unstable contribution to the dihedral effect of the rotorcraft.

The sidewash distribution will in a similar way produce variations in tail rotor thrust and vertical tail surface sideforce with angle of attack. The nature of the effects depend quite significantly upon whether the center of the wake intersects with surface or not. Generally if the wake centerline is centered on the vertical tail there is a strong anti-symmetric distribution and the variation with angle of attack will produce a significant variation in the sideforce of the vertical tail. An increase in angle of attack produces a reduction in sideforce of the tail rotor and consequently a positive yawing moment with increasing angle of attack. As the centerline of the wake moves above the surface the gradient changes quite rapidly as indicated in Figure 5 which shows the variation in average sidewash with angle of attack. This is a source of a significant increase in yawing moment with increase in angle of attack. Loss in dutch roll damping has been attributed to this derivative associated with main rotor torque variations at high speeds [3]. This sidewash effect appears considerably larger than the torque change. This effect taken with the pitching moment variation with slip causes in general a coupling between the short period motion and the dutch roll and a loss in dutch roll damping.

Consider now the tail rotor thrust change with angle of attack due to the sidewash variation. Recall that the influence of the sidewash gradient on the tail rotor will be quite different from the vertical tail because of the weighting of sidewash velocity by tail rotor radius. As a consequence the variation in the weighted sidewash with angle of attack which shows the thrust variation is quite non-linear for the flat wake model as shown in Figure 6. Using the sidewash distribution of Figure 3 there is a significant change in thrust as the horizontal blades encounter the change

in sidewash associated with moving away from the center of the rotor wake. For this distribution the effect of the up and down blades is non-linear. There is a decrease in thrust with increase in angle of attack and consequently a second contribution to the variation in yawing moment with angle of attack further contributing to a reduction in dutch roll stability with increasing airspeed. The sidewash distribution predicted by the free wake model discussed in the next section gives a relatively linear variation as shown in the Figure.

Generally the effects discussed above vary in the following fashion with airspeed. Since the asymmetric component of normalized downwash which gives the primary contribution to the pitching moment variation with slip varies with advance ratio, this stability derivative will vary as,

$$\frac{\partial M}{\partial \beta} \sim \mu^2 \bar{v}_o \sim \frac{\mu C_T}{2}$$

Thus increasing linearly with airspeed. The normalized sidewash is proportional to advance ratio as well and consequently the coupling derivative will vary in a similar fashion,

$$\frac{\partial N}{\partial \alpha} \sim \mu \frac{C_T}{2}$$

It is the combination of these two derivatives that gives rise to a loss in dutch roll stability which has been noted on many contemporary helicopters at high speeds.

Following the next section which discusses the comparison of the simple flat wake model with a more advanced free wake model the influence of these effects on the helicopter response is discussed.

Comparison with Advanced Free Wake Rotor Models

In order to successfully analyze the loads experienced by a helicopter in the presence of the main rotor wake it is necessary to accurately model the effect of the vortex wake of the main rotor. Over the past twenty years, a variety of computational rotor wake models have been developed, largely for application to problems concerning main rotor performance and airloads [8,9,10]. Recently, a new approach to wake modelling has been developed that is superior in many important respects to previous work and has been successfully incorporated into analyses of rotorcraft interactional aerodynamics (Reference 5). This new approach involves using a force-free model of the wake of the full span of each rotor blade.

The fundamental building block of this analysis is the Basic

Curved Element (BCVE), which is derived from the approximate Biot-Savart integration for a parabolic arc filament. When used in conjunction with a scheme to fit the elements along a vortex filament contour, this method has a significant advantage in overall accuracy and efficiency when compared to the traditional approach, which involves the use of straight-line vortex segments. A theoretical and numerical analysis (Reference 11) has shown that free wake flows involving close interaction between filaments should utilize curved vortex elements in order to guarantee a consistent level of accuracy. The curved element method was implemented into a forward flight free wake analysis in Reference 12, featuring a single free tip vortex trailing from each blade, a model similar to many previous forward flight wake treatments. This model exhibited rapid convergence and robust behavior, even at relatively low advance ratio.

In many important forward flight conditions (particularly at high speed), the rotor wake structure can become very complicated, and wake models using a single free tip vortex are inadquate. On the advancing side, the generating blade may experience large spanwise and azimuthal load variations, including negative tip loading; the effects of such distributions will not be correctly captured by relatively crude single-vortex models. The new wake analysis methods described in References 12 and 13 seek to represent the important features of the resulting wake generated along the full span of the blade. Figure 7 shows the new full-span free wake generated by one blade of a four-bladed rotor at advance ratio 0.39. The curved elements are used to represent vortex filaments laid down along contours of constant sheet strength in the wake. The skewed/curved filaments provide a natural representation of the free wake vorticity field, which simultaneously accounts for both shed and trailed vorticity. An additional advantage of the method is that it provides a visually meaningful representation of the wake since the filaments correspond to the actual resultant vorticity field. The vortex filaments leaving the blade in Figure 7 are all of constant strength, and each one is of equal value. For this reason, close spacing between filaments implies a strong net influence from that region of the wake, whereas a sparse spacing indicates a region of having little effect. The looping (or connecting) between outboard and inboard filaments is associated with changes in the maximum bound circulation on the blade. A strong root vortex structure is also evident. The actual aerodynamic environment experienced by the regions immersed in this complex wake structure can be inferred from Figure 7. From the standpoint of resolving the flow in the vicinity of the empennage, these wake geometry plots show a remarkably complicated incident wake structure.

This free wake model has been applied to the problem of the prediction of vibratory loads on the main rotor (Reference 13), the analysis of high-resolution flow fields for tail rotor aeroacoutics (Reference 14), and to the effects of the

interaction of the rotor wake with downstream fuselage and empennage surfaces (Reference 5). The latter application is clearly the one most directly related to the topics under consideration here. In Reference 5, very encouraging correlation was found between measurements the time-average flow field downstream of an AH-64 wind tunnel model at advance ratio 0.28 and predictions made using the full-span wake model just described (see Figure 8, part of which was taken from Reference 15). In view of these results, it was naturally of interest to examine the correlation between the predictions made by the full-span free wake model and the flat wake model described above. The full-span model has been successfully applied for research on a variety of topics in rotor aerodynamics, but is on the whole too computationally demanding for routine use in studies of handling qualities. Thus, it is desirable to see if the flat wake representation can capture the major features of the wake effect on empennage surfaces downstream of the rotor.

Sample calculations were performed using an isolated UH-60 main rotor at advance ratio 0.2, operating at a specified thrust coefficient. The shaft angle of attack and the blade pitch were set at values corresponding to the desired forward flight trim condition. In the current free wake analysis, a vortex lattice model of the blade is used, along with a relatively simple blade dynamics model featuring rigid flapping and one elastic bending mode. A trim routine is coupled to the blade dynamics analysis to ensure that the pitch control inputs to the blade are consistent with zero net hub moment.

For flow field computations, a measurement grid is set up downstream of the main rotor, and the predicted velocity field is computed and stored at each time step. For these calculations, sixteen time steps per main rotor azimuth were used. Since the wake analysis starts assuming an undistorted, kinematic wake, typically several rotor revolutions of simulated time must elapse before the calculation reaches a repeatable steady state. Once such a state is achieved, the velocity field at the measurement grid is time-averaged and normalized; these results can then be directly compared with the flat wake predictions.

The first calculation undertaken here featured the UH-60 operating at a thrust coefficient of 0.007 and a shaft angle of attack of -5 deg. The plots in Figures 9 and 10 show the comparisons of downwash and sidewash predicted by the flat wake and free wake models at the vertical level corresponding to the horizontal stabilizer position. As is evident, the predicted velocity fields are qualitatively quite similar and also show considerable quantitative similarities except in the peak values on the advancing side. One possible explanation for this dissimilarity is the different treatments of the blade bound circulation in the two cases. The flat wake calculation assumes a simple cubic bound circulation

distributions whose magnitude is proportional to the momentum theory value of downwash and which is invariant with azimuth angle. The free wake calculation computes the spanwise circulation distribution for each azimuth angle that satisfies the flow tangency conditions at the blade surface. Clearly, this could lead to substantially different bound circulation distributions, which could in turn produce significant changes in the flow field downstream.

To quantify the differences in the bound circulation, the time-averaged circulation for the free wake calculation was valued and is shown in Figure 11. The distributions show considerable differences near the root and the tip, and the peak level of average circulation is substantially lower in the free wake case than in the flat wake case. The flat wake value is roughly 15% higher than the free wake prediction; since the flat wake velocity field scales with the maximum bound circulation, reducing the flat wake input to match the peak spanwise level in the free wake calculation would improve the agreement considerably. The deviation of the bound circulation from the assumed cubic distribution would also effect the predicted velocity field; thus, it would probably be desirable to adjust the spanwise circulation distribution to be more representative of actual load distributions in follow-on applications of the flat wake model. Nonetheless, the agreement for this case (at relatively high forward speed) is quite encouraging, particularly the downwash in the immediate vicinity of the horizontal stabilizer position ($\bar{z} = -0.25$ to 0.25).

An additional calculation was undertaken to compare the vertical distribution of sidewash experienced by the tail rotor and vertical tail for this same flight condition. The results for both the free wake and flat wake cases are shown in Figure 12. Note that the free wake result does not display the symmetry of the flat wake case, though it does tend to reduce the peak levels of sidewash that are observed. Also, though the vertical gradient of sidewash is steep even in the free wake case, it is somewhat "softened" relative to the abrupt jump evident in the flat wake results of Figure 3.

Comparison With Flight Test

Using the methods described in the previous section the influence of the aerodynamic characteristic of the interaction of the rotor wake with the flow field the linearized contribution to the stability derivatives are calculated and use in a linearized model of the complete rotorcraft dynamics including the rotor and body states as well as the dynamic inflow. This model is described in detail in Reference 6. A simpler version of the wake flow field was used in Reference 6 to compare predicted responses with flight test. Since the primary effect of lateral longitudinal coupling terms discussed above influence the rudder response, only this control response is discussed. Figures 12 and 13 show the

left and right rudder responses using different linearized coupling terms. These are considerably longer time responses then were available for the study of Reference 6. Case 1 corresponds to the very simple free wake model used in Reference 6. The downwash is the far downstream value in the plane of the wake. This approximation gives the largest values for the coupling derivatives, the rate of change of pitching moment with slip and the yawing moment change with angle of attack. It can be seen from the responses that this level of coupling over estimates the coupling and in fact produces an unstable dutch roll mode. The first pitch rate peak is accurately estimated. This peak is directly dependent upon the value of the pitching moment variation with slip. Case 2 is based on the more accurate version of the flat wake model described in the paper. This reduces the coupling levels although still the dutch roll damping is too low. Case 3 uses the values from the free wake model and tends to give better agreement although the dutch roll damping is underestimated. The free wake model also appears to underestimate the pitch sideslip coupling. Generally the roll axis correlation is poor. The roll axis is sensitive to a variety of terms due to the low level of the roll inertia, although in general the predicted amplitude of the roll rate response is significantly in error. It seems quite possible that the non-linearities shown in the aerodynamic behavior may be responsible for this behavior, as well as perhaps the difficulty in calculating the changes in aerodynamic forces due to the high gradients in velocity components shown. Further studies are in progress to examine these effects in more detail.

3. Conclusions

1.) The general features of the time-averaged flow field downstream of the main rotor can be estimated by a relatively simple flat wake model.

2.) A more accurate free wake calculation of the downstream flow field shows considerable similarity to the flat wake model predictions at reasonable translational speeds.

3.) The lateral distribution of downwash across the horizontal tail gives rise to a pitching moment variation with sideslip. The vertical distribution of sidewash across the vertical tail and tail rotor gives rise to yawing and rolling moment variations with angle of attack.

4.) Estimation of the coupling derivatives from the flat wake model appears to overestimate the coupling effects. Use of the free wake model to estimate these effects gives reasonable correlation with flight test control responses.

4. Acknowledgement

Part of this research was supported by NASA Ames Research Center, Grant No. NAG 2-561. The development of the free wake analysis used here was supported by the U. S. Army Research Office.

5. References

1) D. E. Cooper, YUH-60A Stability and Control, Journal of the American Helicopter Society, Vol. 23, No. 3, July 1978.

2) V. E. Baskin, et al., Theory of the Lifting Airscrew, NASA TT F-823, 1976.

3) K. B. Amer, R. W. Prouty and R. P. Walton, Handling Qualities of the Army/Hughes YAH-64 Advanced Attack Helicopter, AHS Preprint 78-31, paper presented at the 34th Annual Forum of the AHS, Washington, DC, May 1978

4) R. W. Prouty, Importance of Aerodynamics on Handling Qualities, Paper presented at the AHS Specialists' Meeting on Aerodynamics and Aeroacoustics, Arlington, TX, February 25-27, 1987.

5) T. R. Quackenbush, and D. B. Bliss, Free Wake Prediction of Rotor Flow Fields for Interactional Aerodynamics, Proceedings of the 44th Annual Forum of the AHS, June 1988.

6) H. C. Curtiss, Jr. and R. M. McKillip, Jr., Studies in Interaction System Identification of Helicopter Rotor/Body Dynamics Using an Analytically-Based Lower Model, Paper presented at the International Conference on Helicopter Handling Qualities and Control, London, UK, November 1988.

7) M. G. Ballin, Validation of a Real-Time Engineering Simulation of the UH-60A Helicopter, NADA TM 88360, February 1987.

8) M. P. Scully, Computation of Helicopter Rotor Wake Geometry and Its Influence on Rotor Harmonic Airload, Massachusetts Institute of Technology Aeroelastic and Structures Research Laboratory, ASRL TR 178-1, March 1975.

9) T. A. Egolf, and A. J.Landgrebe, Helicopter Rotor Wake Geometry and Its Influence in Forward Flight, Vols., I and II, NASA CR 3726 and 3727, October 1983.

10) S. G. Sadler, Main Rotor Free Wake Geometry Effects on Blade Air Loads and Response for Helicopters in Steady Maneuvers, NASA CR 2110 and 2111, September 1972.

11) D. B. Bliss, M. E. Teske, and T. R. Quackenbush, A New Methodology for Free Wake Analysis Using Curved Vortex Elements, NASA CR 3958, 1978.

12) D. B. Bliss, L. U. Dadone, and D. A. Wachspress, Rotor Wake Modelling for High Speed Applications, Proceedings of the 43rd Annual Forum of the AHS, May 1987.

13) T. R. Quackenbush, D. B. Bliss, and D. A. Wachspress, Preliminary Development of an Advanced Free Wake Analysis of Rotor Unsteady Airloads, Final Report to NASA/Ames under Contract NAS2-12554, August 1987.

14) T. R. Quackenbush, D. B. Bliss, and A. Mahajan, High Resolution Flow Field Predictions for Tail Rotor Aeroacoustics, Proceedings of the 45th Annual Forum of the AHS, May 1989.

15) A. H. Logan, R. W. Prouty, and D. R. Clark, Wind Tunnel Tests of Large- and Small-Scale Rotor Hubs and Pylons, USAAVRADCOM TR-80-D-21, April 1981.

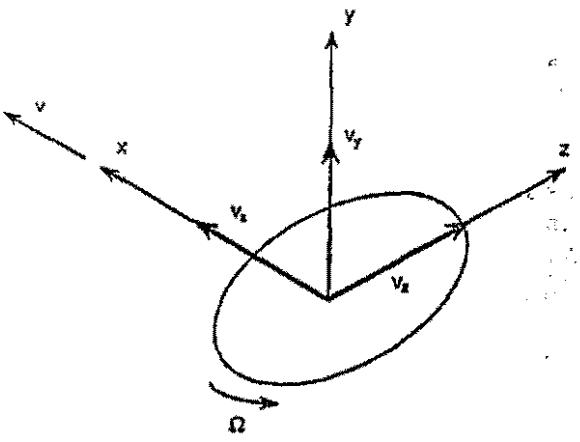

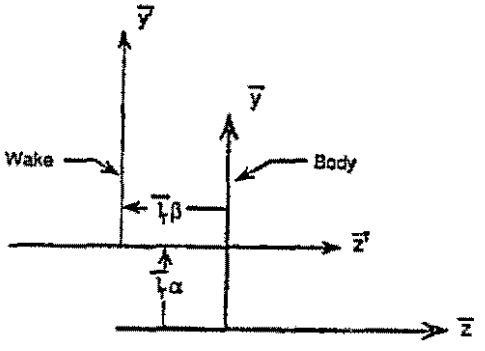

Fig. 1: Coordinate System

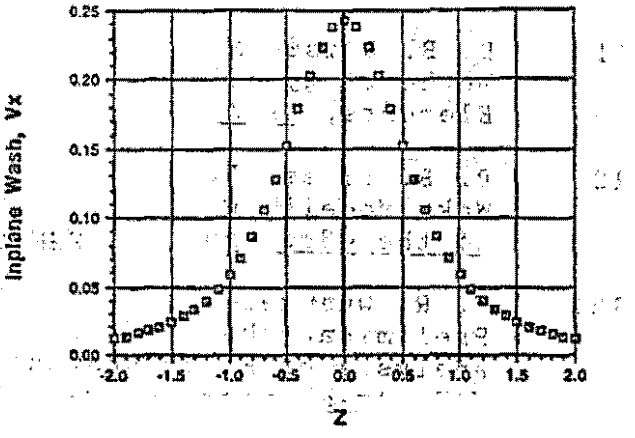

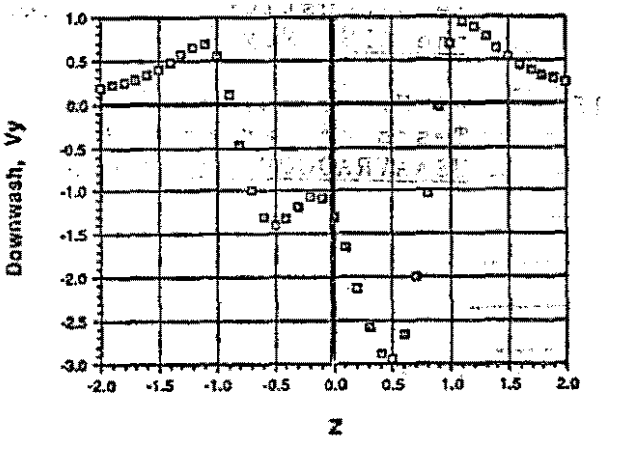

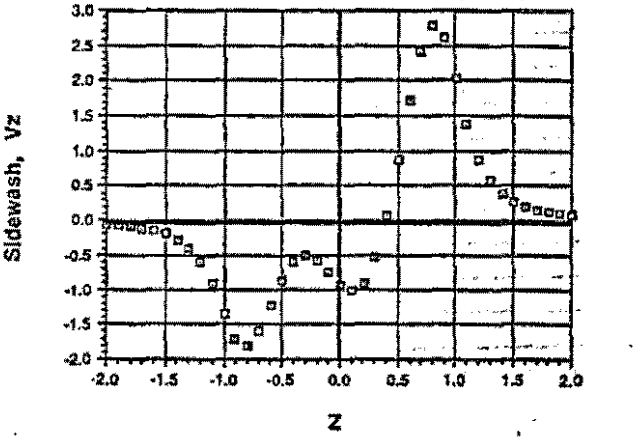

Fig. 2: Lateral Distribution of Normalized Wake Velocities at Horizontal Tail Location (x = -1.1, y = - .22) at an advance ratio = 0.2. Flat Wake.

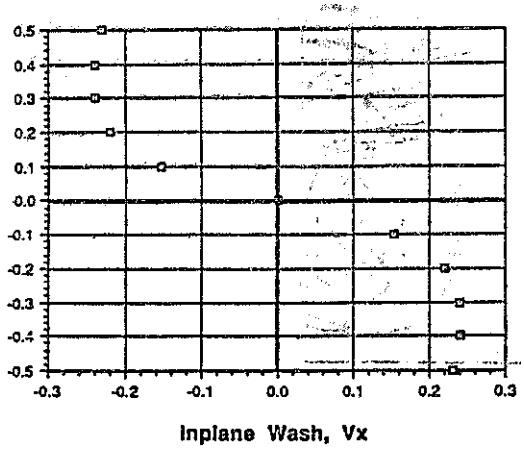

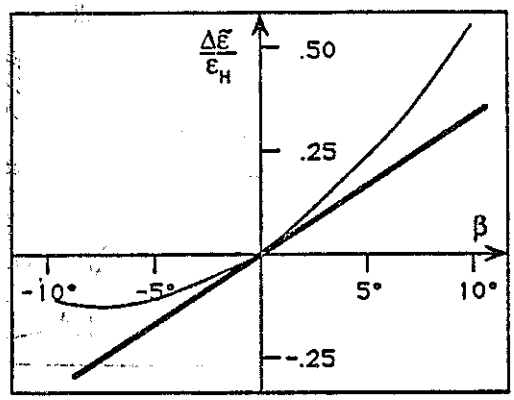

Fig. 4: Horizontal Tail. Weighted Downwash Variation with Sideslip.

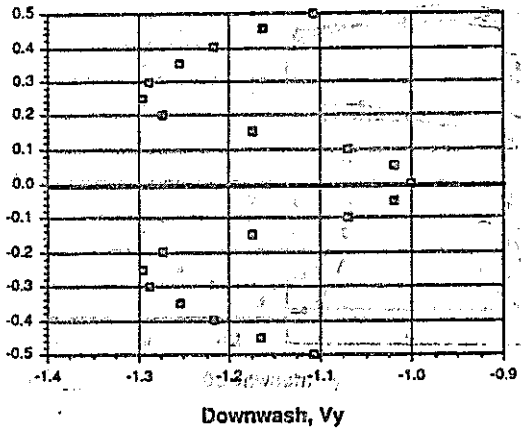

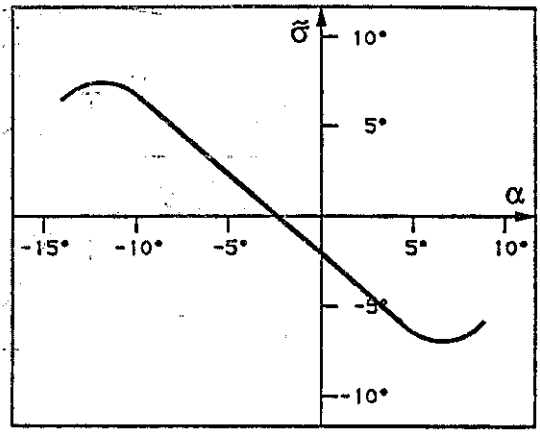

Fig. 5: Vertical Tail. Weighted Sidewash Variation with Angle of Attack.

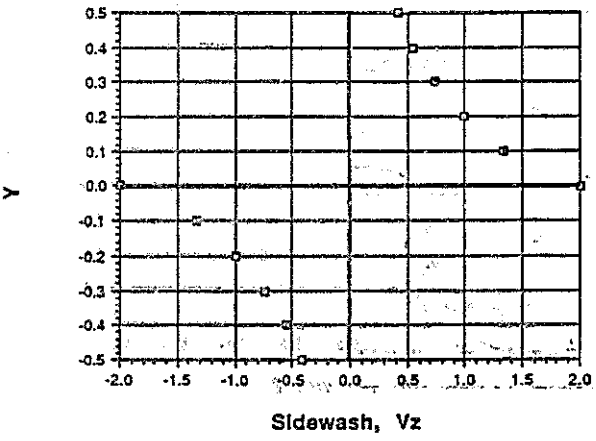

Fig. 3: Vertical Distribution of Normalized Wake Velocities at Tail Location ($x = -1.1$, $z = 0.0$) at an Advance Ratio = 0.2. Flat Wake.

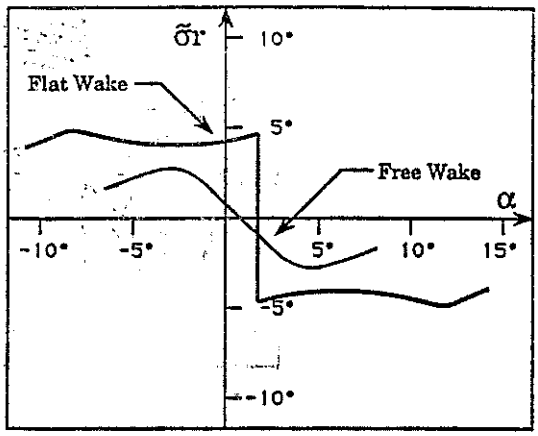

Fig. 6: Tail Rotor. Radius Weighted Sidewash Variation with Angle of Attack.

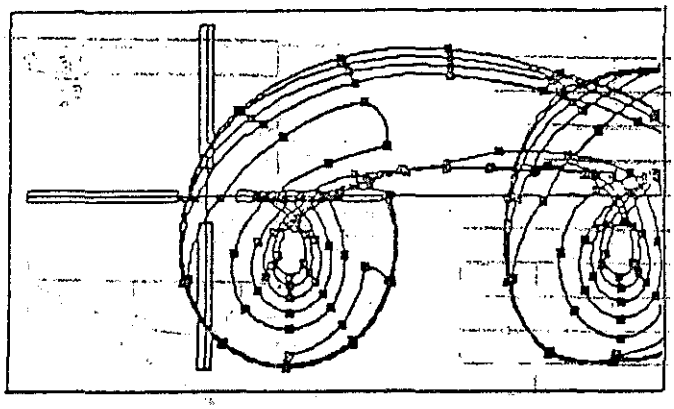

a) $\psi = 0°$

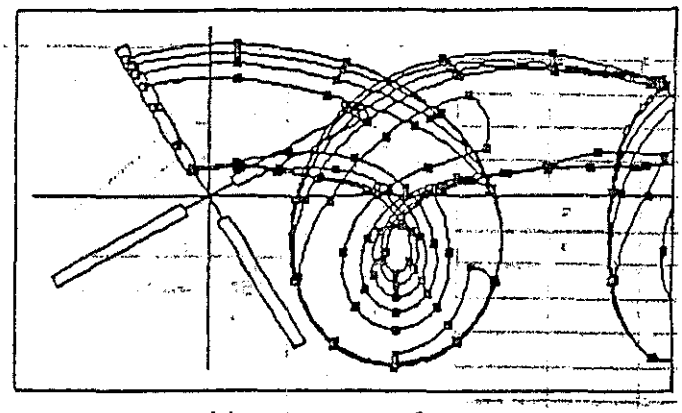

b) $\psi = 120°$

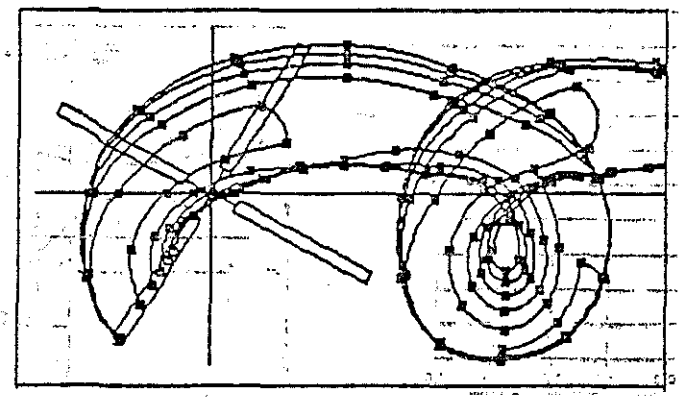

c) $\psi = 240°$

Fig. 7: Full-Span Free Wake Geometry for a Four-Bladed AH-64 Main Rotor in Forward Flight At Advance Ratio 0.28.

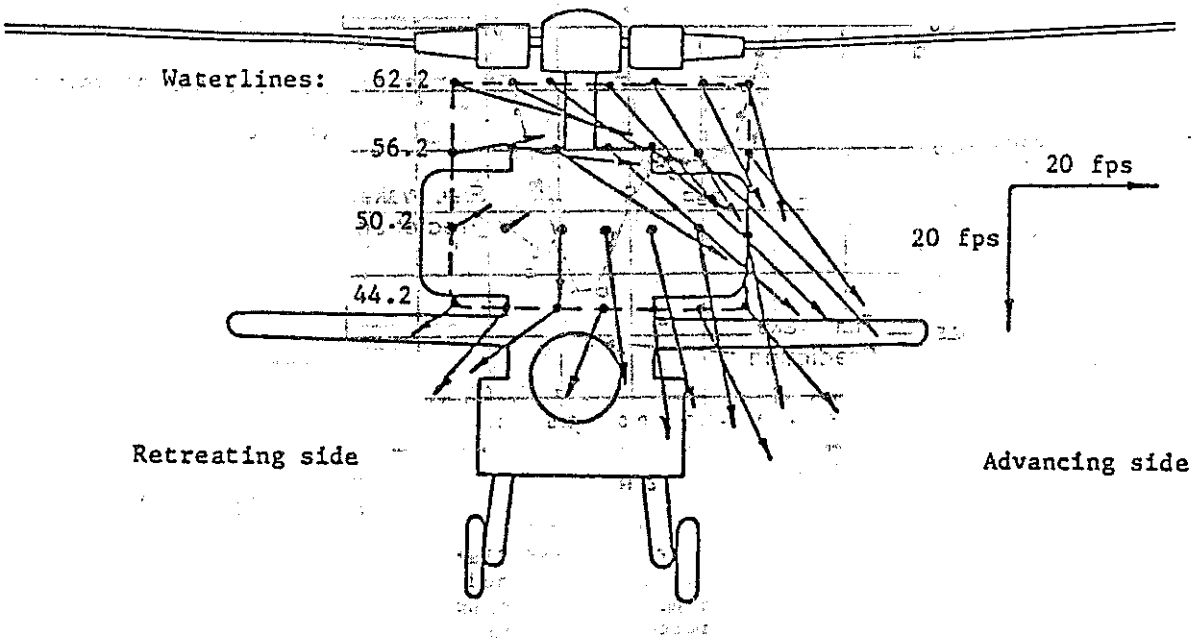

Fig. 8: a) Crossflow Velocities for the AH-64 Wind Tunnel Model, (x = -1.3). Advance ratio 0.28 (from Reference 15.

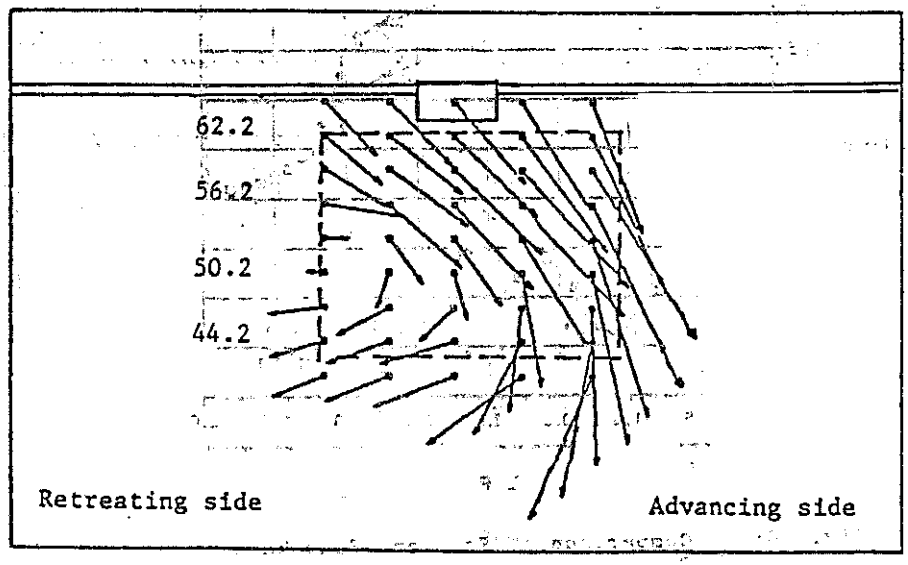

b) Free Wake Prediction of a) Identical Scales.

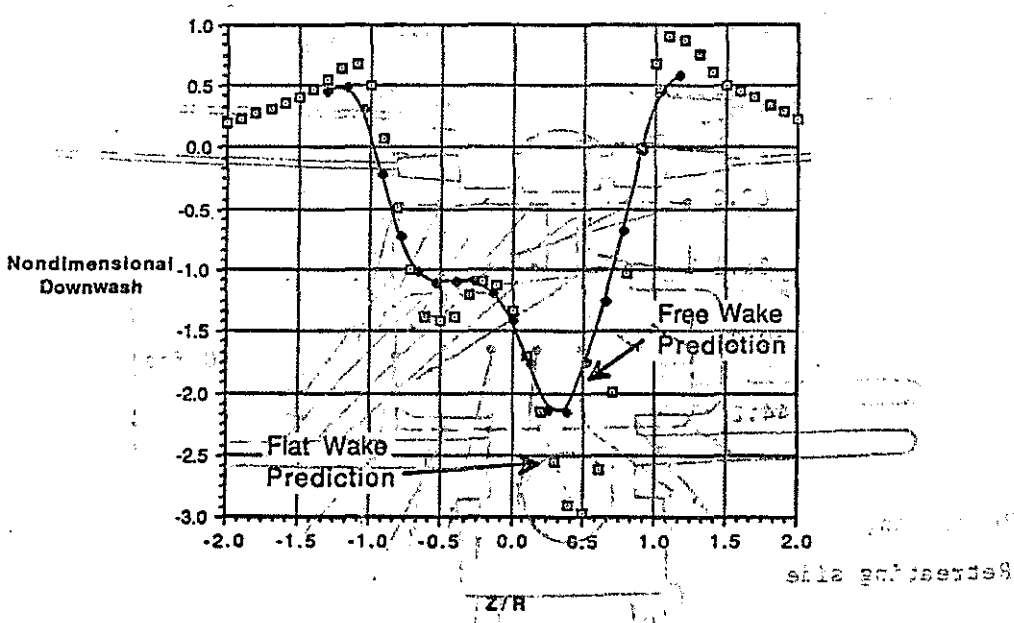

Fig. 9: Comparison of Free and Flat Wake Predictions for Normalized Downwash at Horizontal Stabilizer Location UH-60. Advance Ratio = 0.2.

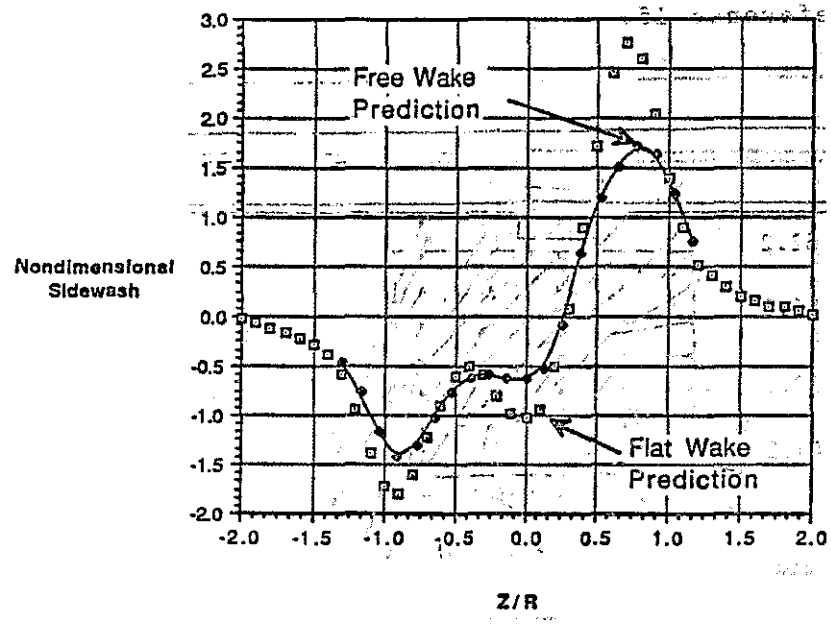

Fig. 10: Comparison of Free and Flat Wake Predictions for Normalized Sidewash Distribution at Horizontal Stabilizer Location, UH-60, Advance Ratio = 0.2.

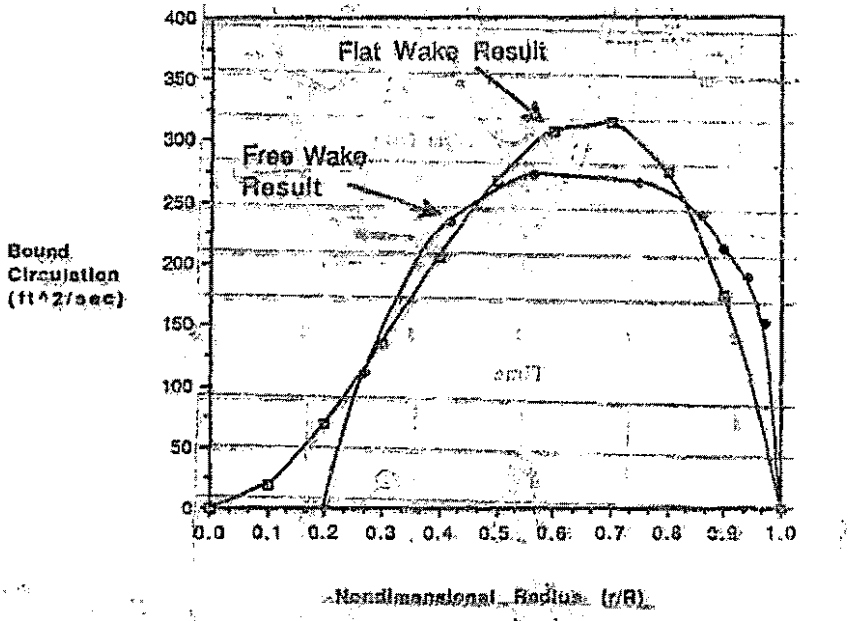

Fig. 11: Comparison of Average Bound Circulation Distribution UH-60. Advance Ratio 0.2, Thrust Coefficient .007.

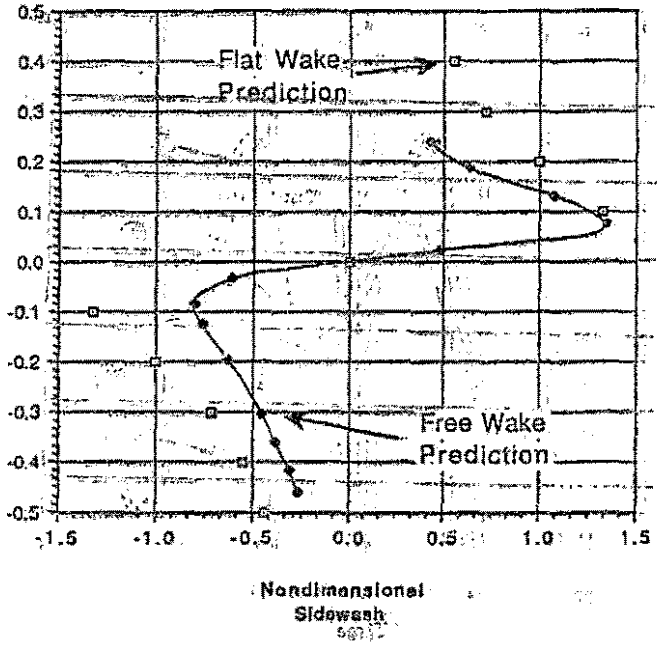

Fig. 12: Comparison of Free and Flat Wake Prediction for Normalized Vertical Distribution of Sidewash, UH-60, Vertical Tail Location.

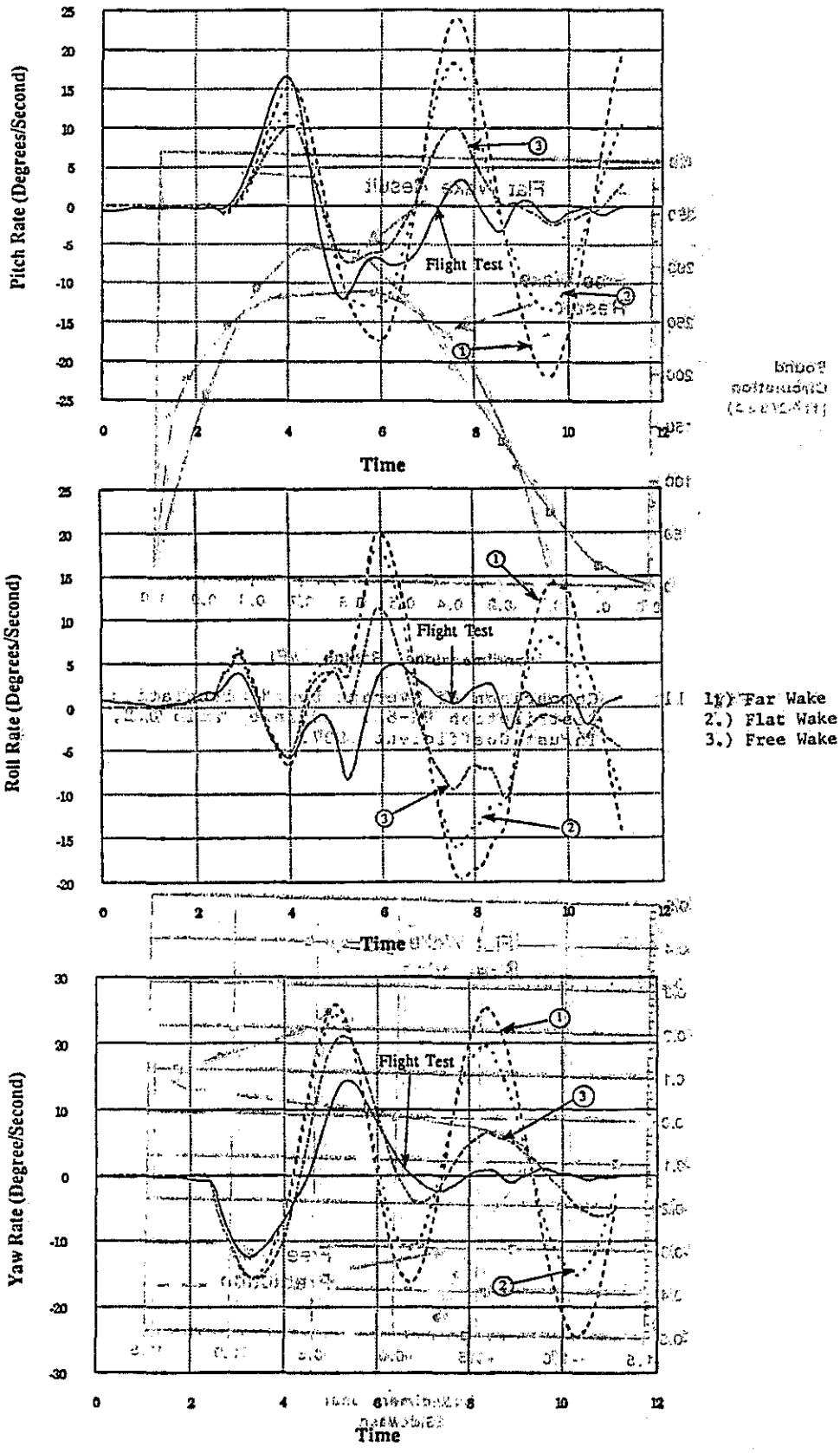

Fig. 13: Comparison of Theory and Experiment. Coupling Derivatives from Various Wake Models. UH-60 Left Pedal Response 100 kts.

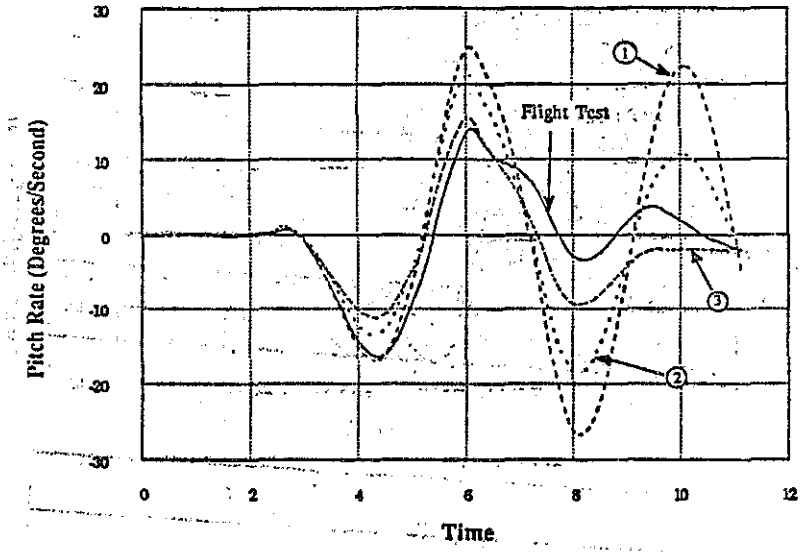

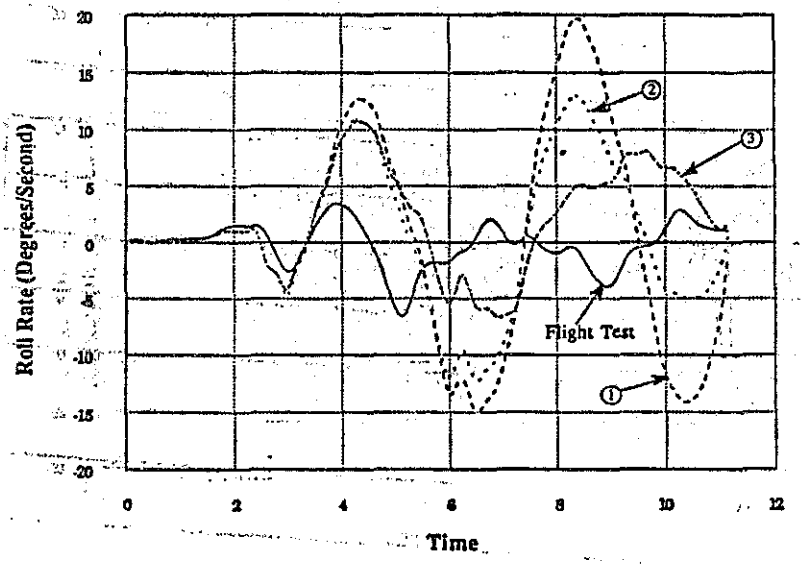

1.) Far Wake
2.) Flat Wake
3.) Free Wake

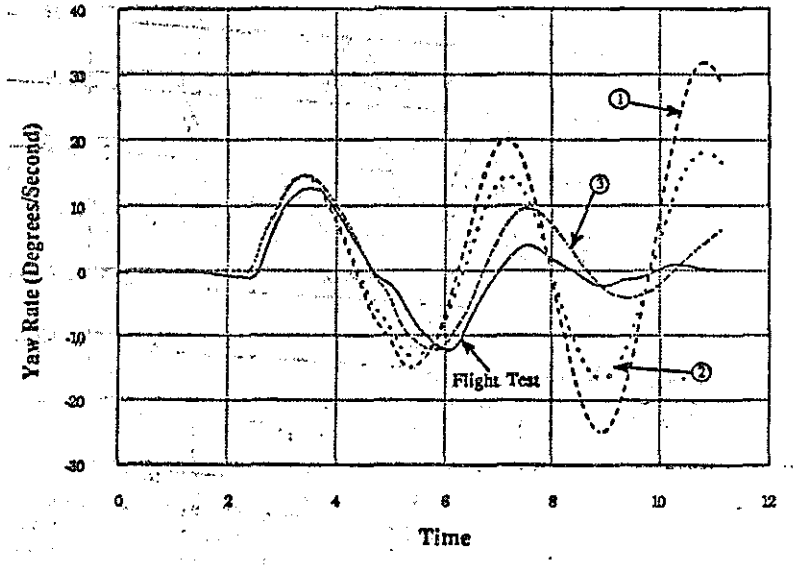

Fig. 14: Comparison of Theory and Experiment. Coupling Derivatives from Various Wake Models. UH-60A Right Pedal Response 100 kts.